

First-principles calculations of exchange interactions, spin waves, and temperature dependence of magnetization in inverse-Heusler-based spin gapless semiconductors

A. Jakobsson^{1,2,*}, P. Mavropoulos^{2,†}, E. Şaşıoğlu^{2,‡}, S. Blügel², M. Ležaić², B. Sanyal¹, and I. Galanakis^{3§}

¹*Department of Physics and Astronomy, Uppsala University, Box 516, 75120 Uppsala, Sweden*

²*Peter Grünberg Institut and Institute for Advanced Simulation, Forschungszentrum Jülich and JARA, 52425 Jülich, Germany*

³*Department of Materials Science, School of Natural Sciences, University of Patras, GR-26504 Patra, Greece*

Employing first principles electronic structure calculations in conjunction with the frozen-magnon method we calculate exchange interactions, spin-wave dispersion, and spin-wave stiffness constants in inverse-Heusler-based spin gapless semiconductor (SGS) compounds Mn_2CoAl , Ti_2MnAl , Cr_2ZnSi , Ti_2CoSi and Ti_2VAs . We find that their magnetic behavior is similar to the half-metallic ferromagnetic full-Heusler alloys, i.e., the intersublattice exchange interactions play an essential role in the formation of the magnetic ground state and in determining the Curie temperature, T_c . All compounds, except Ti_2CoSi possess a ferrimagnetic ground state. Due to the finite energy gap in one spin channel, the exchange interactions decay sharply with the distance, and hence magnetism of these SGSs can be described considering only nearest and next-nearest neighbor exchange interactions. The calculated spin-wave dispersion curves are typical for ferrimagnets and ferromagnets. The spin-wave stiffness constants turn out to be larger than those of the elementary $3d$ -ferromagnets. Calculated exchange parameters are used as input to determine the temperature dependence of the magnetization and T_c of the SGSs. We find that the T_c of all compounds is much above the room temperature. The calculated magnetization curve for Mn_2CoAl as well as the Curie temperature are in very good agreement with available experimental data. The present study is expected to pave the way for a deeper understanding of the magnetic properties of the inverse-Heusler-based SGSs and enhance the interest in these materials for application in spintronic and magnetoelectronic devices.

PACS numbers: 75.47.Np, 75.50.Cc, 75.30

I. INTRODUCTION

Heusler compounds and alloys are a huge family of intermetallic compounds^{1,2} and they owe their name to the German metallurgist Friedrich Heusler who in 1904 studied the thermodynamic properties of Cu_2MnAl .³ The development of the research fields of magnetoelectronics and spintronics⁴ intensified the interest in the half-metallic Heusler compounds.^{5–7} In half-metallic magnets a metallic majority-spin electronic band structure and a semiconducting minority-spin electronic band structure coexist.^{8,9} Such compounds could lead to the creation of a fully spin-polarized current, maximizing the efficiency of spintronic devices.¹⁰ In addition, half-metallicity in Heusler compounds is always accompanied by the so-called Slater-Pauling rule where the total spin magnetic moment scales linearly with the number of valence electrons in the unit cell.^{11–16} Although a large number of half-metallic Heusler compounds has been studied, still novel properties are discovered among Heusler alloys, e.g. ferromagnetic or ferrimagnetic semiconducting behavior,^{17–20} paving the way for diverse applications in spintronics/magnetoelectronics.²¹

A class of materials bridging the gap between half-metals and magnetic semiconductors are the so-called spin-gapless semiconductors (SGS); magnetic semiconductors where there is an almost zero-width energy gap at the Fermi level in the majority-spin direction and a usual energy gap in the other spin-direction.²² In SGS (i) the mobility of carriers is considerably larger than in

usual semiconductors, (ii) excited carriers include both electrons and holes which can be 100% spin-polarized simultaneously, and (iii) a vanishing amount of energy is enough to excite majority-spin electrons from the valence to the conduction band. Several compounds have been identified as SGS,^{23–31} and among them exist a few Heusler compounds,^{16,32–35} and it is Mn_2CoAl , an inverse full-Heusler compound, which has attracted most of the attention due to its successful growth in the form of films. First in 2008 Liu and collaborators synthesized using an arc-melting technique Mn_2CoAl and found that it adopted the lattice structure of inverse full-Heuslers (see Fig. 1 for a schematic representation of the structure) with a lattice constant of 5.8388 Å and a total spin magnetic moment of 1.95 μ_B per formula unit.³⁶ The lattice of inverse Heuslers is known as the XA (or X_α)-structure and it is similar to the well-known $L2_1$ structure of full Heusler compounds like Co_2MnAl where only the sequence of the atoms in the unit cell changes. Moreover electronic structure calculations yielded a ferrimagnetic state with a total spin magnetic moment of 1.95 μ_B per formula unit and an antiparallel coupling between the Mn nearest-neighboring atoms.³⁶ Although the calculated structure in Ref. 36 is that of a SGS, authors do not mention it in their article.³⁶ In 2011 Meinert and collaborators studied again theoretically this compound and almost reproduced the calculated results of Liu *et al.* using a different electronic structure method.³⁷ They have also calculated the exchange constants showing that they are short range and the magnetic state is

stabilized mainly due to the direct interaction between nearest-neighbors and predicted a Curie temperature of 890 K.³⁷ But it was not until 2013, when Ouardi et al identified the SGS behavior of Mn_2CoAl and have confirmed it experimentally in bulk-like polycrystalline films.³⁸ The experimental lattice constant was found to be 5.798 Å, the Curie temperature was measured to be about 720 K and the total spin magnetic moment per formula unit was found $2 \mu_B$ at a temperature of 5 K.³⁸ Following this research work, Jamer and collaborators have grown thin films of 70nm thickness on top of GaAs,³⁹ but these films were found to deviate from the SGS behavior.⁴⁰ On the contrary, films -grown on top of a thermally oxidized Si substrate- were found to be SGS with a Curie temperature of 550 K.⁴¹ First-principles calculations of Skaftouros et al identified among the inverse Heusler compounds four additional potential SGS materials: Ti_2CoSi , Ti_2MnAl , Ti_2VAs and Cr_2ZnSi , the latter three being also fully-compensated ferrimagnets, and V_3Al for which one V sublattice is not magnetic and the other two form a conventional antiferromagnet.³² The SGS character of Ti_2MnAl was also confirmed by Jia *et al.*⁴² Wollman *et al.*⁴³ confirmed the conclusion of Meinert *et al.* that direct exchange interactions are responsible for the magnetic order in Mn_2CoAl studying a wide range of Mn_2 -based Heusler compounds and predicted a Curie temperature of 740 K using the spherical approximation.⁴⁴ Skaftouros *et al.* have discussed in detail the behavior of the total magnetic moment in inverse Heusler compounds including the SGS materials.¹⁴ Galanakis and collaborators have shown that defects keep the half-metallic character of Mn_2CoAl but destroy the SGS character.⁴⁵ Finally, recent studies on the effect of doping of Mn_2CoAl with Co, Cu, V and Ti,⁴⁶ as well as the anomalous Hall effect have appeared in literature.⁴⁷

Motivated by these recent advances in SGS systems, the present work aims at a prediction and understanding of their magnetic properties at elevated temperatures. We employ density-functional theory at the ground state augmented by a Heisenberg model Hamiltonian for the prediction of the temperature dependent magnetization.

We present calculations of exchange interactions, spin waves and temperature dependence of the magnetization in five inverse Heusler compounds known to present spin-gapless semiconducting behavior studied in Ref. 32: Mn_2CoAl , Ti_2CoSi , Ti_2MnAl , Ti_2VAs and Cr_2ZnSi . We find that magnetic behavior of the SGSs is similar to the half-metallic ferromagnetic full-Heusler alloys, i.e., the intersublattice exchange interactions play an essential role in the formation of the magnetic ground state and in determining the critical temperature, T_c . Note, that even in the case of zero total spin magnetic moment in the unit cell, the compounds under study are fully-compensated ferrimagnets and not conventional antiferromagnets, and thus the critical temperature should be called “Curie temperature” and not “Néel temperature”. It turns out that the T_c of all compounds is much above the room temperature. The calculated magnetiza-

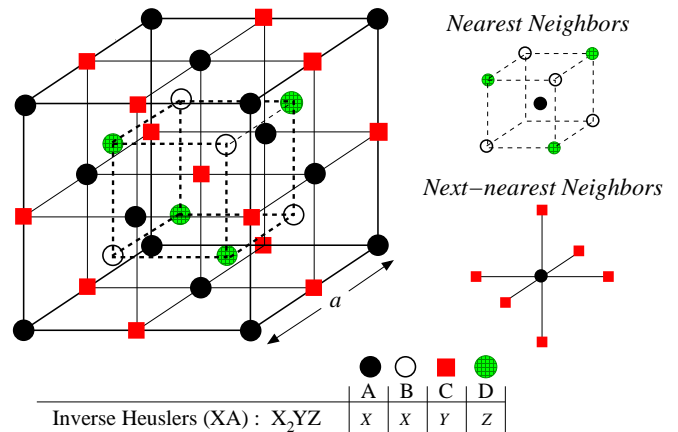


FIG. 1: Schematic representation of the lattice structure of inverse Heusler compounds having the chemical formula X_2YZ where X and Y are transition metal atoms (with the valence of Y larger than of X) and Z is an sp-element. On the right we present the nearest and next-nearest neighbors of an A site. Note that the large cube contains exactly four primitive unit cells.

tion curve for Mn_2CoAl as well as the Curie temperature are in very good agreement with available experimental data. The rest of the paper is organized as follows: In Sec. II we present the computational method. In Sec. III we present the computational results, and Sec. III gives the conclusions.

II. COMPUTATIONAL METHOD

A. Crystal structure and ground state calculations

Prior to discussing the structure of the compounds under study, we should note that Mn_2CoAl has been already synthesized experimentally,³⁸ and for the other four compounds one should calculate the formation enthalpy to establish their possible experimental existence. In Refs. 13 and 15, authors studied the formation enthalpies for 810 Heusler compounds and concluded that the formation of the compounds is not favored with respect to the constituent elements only in the case where the heavier main-group metals such as thallium, lead and bismuth are involved. Thus we expect the compounds under study to be thermodynamically stable.

All five compounds under study are called inverse Heuslers and crystallize in the so-called XA or X_α structure, the prototype of which is CuHg_2Ti , but usually the sequence of the atoms follows the chemical formula X_2YZ . X and Y are transition metal atoms with the valence of X being smaller than Y, and Z is a sp atom. A schematic representation of the structure is given in Fig. 1. There are four atoms along the diagonal of the cube following the sequence X-X-Y-Z and thus the two X atoms sit at sites of different symmetry. We use the superscripts A and B to distinguish them. As

shown also in the figure, each atom at the A or C site resides at the center of a cube with nearest neighbors four B sites and four D sites sitting at the corners of the cube; equivalently each atom at a B or D site has four atoms at A sites and four atoms at C sites as nearest neighbors. Concerning the next-nearest neighbors each A site has as second neighbors six C sites (and each C site has six A sites as second neighbors), and equivalent is the situation for the B and D sites. The environment of each site is important for the discussion of the magnetic properties of these compounds. We have used the lattice constants determined in Ref. 32 using the full-potential nonorthogonal local-orbital minimum-basis band structure scheme (FPLO)⁴⁹ with the GGA exchange-correlation potential.⁵⁰ For Mn₂CoAl the calculated value of 5.73 Å is slightly smaller than the experimentally determined lattice constants of 5.8388 and 5.798 Å in Refs. 36 and 38, respectively. We compute the ground state electronic properties using the full-potential linearized augmented plane wave (FLAPW) method as implemented in the FLEUR code⁵¹ combined with the generalized gradient approximation (GGA) to the exchange-correlation potential as parameterized by Perdew *et al.*⁵⁰

B. Exchange constants and spin-wave dispersion

Next we present the formalism on which the calculations of the exchange constants are based. Our starting point is the classical Heisenberg model with unit vectors $\mathbf{e}_{n\alpha}$, pointing along the spin moments at positions $\mathbf{R}_{n\alpha}$ specified by a cell index n and magnetic lattice index α . The spin moments interact via exchange coupling parameters $J_{mn}^{\alpha\beta}$ and the exchange Hamiltonian H_{ex} is

$$H_{ex} = -\frac{1}{2} \sum_{mn\alpha\beta} J_{mn}^{\alpha\beta} \mathbf{e}_{m\alpha} \cdot \mathbf{e}_{n\beta} \quad (1)$$

Note that the magnitude of the moments is incorporated in the parameters J . The exchange parameters are extracted by a least square fit from ab-initio total energy calculations performed using the FLEUR code for a set of spin spirals with randomized wave-vectors.⁵¹ To reduce the computational cost we do non-self consistent calculations and apply the approximation based on the magnetic force theorem^{52,53} to obtain the total energy differences from the differences in sums of eigenvalues.

In order to obtain the adiabatic magnon dispersion,⁵⁴⁻⁵⁷ we set up the spin-wave dynamical matrix $\Delta(\mathbf{q})$ at a Brillouin zone point \mathbf{q} and solve for eigenvalues which provides the magnon frequencies:

$$\Delta_{\alpha\beta}(\mathbf{q}) = 2 \left(\delta_{\alpha\beta} \sum_{\gamma} \frac{J^{\alpha\gamma}(\mathbf{0})M_{\gamma}}{|M_{\gamma}||M_{\alpha}|} - \frac{J^{\alpha\gamma}(\mathbf{q})M_{\beta}}{|M_{\beta}||M_{\alpha}|} \right) \quad (2)$$

$$J^{\alpha\beta}(\mathbf{q}) = \sum_n J_{0n}^{\alpha\beta} \cos[\mathbf{q} \cdot (\mathbf{R}_{0\alpha} - \mathbf{R}_{n\beta})] \quad (3)$$

Here M_{α} is the integrated magnetic moment of sublattice α . In order to obtain the spin-stiffness D of the compounds we fit a linear or quadratic form $D|\mathbf{q}|$ or $D|\mathbf{q}|^2$ respectively to the adiabatic magnon energies along a high symmetry line in the neighborhood of the Γ -point (in cubic systems, D is isotropic). A linear behavior is present for the conventional antiferromagnets and we find it here for the compensated ferrimagnets. We should also note that within our formalism, where we consider an adiabatic approach for the magnons, we cannot study the Landau damping of the spin-waves induced by electron-hole excitations. In the compounds under study we expect the adiabatic approximation to provide reasonable results since there is a Stoner gap separating the magnon spectra from the continuum Stoner excitation spectra as in most half-metallic magnets (with the exception when the Fermi level is exactly at the higher energy edge of the minority-spin energy gap).

C. Temperature dependence of the magnetization and T_c

We employ the classical Monte Carlo technique to calculate the temperature dependence of the magnetization that is derived from the Heisenberg exchange Hamiltonian (1). The technique provides an excellent estimation of the critical temperature, T_c^{MC} , from the position of the peak of the susceptibility as a function of temperature calculated as $\chi(T) = [\langle M^2(T) \rangle - \langle M(T) \rangle^2] / k_B T$, where $\langle \dots \rangle$ denotes thermal averaging over Monte Carlo steps, $M(T)$ is the magnetization (before averaging), and k_B is the Boltzmann constant. Use of a correction for finite-size effects, e.g. the fourth-order cumulant method,⁷¹ can give a more accurate estimation of the critical temperature, but the correction here is small (of the order of a few K) since we are using large simulation supercells ($12 \times 12 \times 12$ primitive cells corresponding to 5184 magnetic atoms). We employ the Metropolis algorithm⁴⁸ and as a random number generator we use the Mersene Twister.⁷² The input comprises both the inter-sublattice and intra-sublattice exchange constants considering only the magnetic atoms, neglecting any contribution due to the interaction of the low-moment sp atoms. Moreover we ignore the contribution of the interstitial region.⁷³

From the exchange constants the Curie critical temperature T_c can be also estimated within the mean-field approximation (MFA). Actually, the critical temperature is given by the average value of the magnon energies which in MFA is the arithmetic average taking all the magnon values with equal weight. Thus is an arithmetic property that the MFA estimation is larger than experimental values⁵⁸⁻⁶⁰. The MFA expression of the critical temperature for a multi-sublattice material like Heusler compounds has been provided in literature.^{61,62}

TABLE I: Calculated atom-resolved and total spin magnetic moments (in μ_B) for the five spin-gapless semiconducting inverse Heusler compounds under study having the chemical formula X_2YZ . The superscripts A and B distinguish the two inequivalent X atoms; we present the sum of the Z spin moment and the interstitial spin magnetic moments; *abs* stands for the sum of the absolute atomic spin magnetic moments. Note that we have used the equilibrium lattice constants as calculated in Ref. 32.

Compound	$a(\text{\AA})$	$m_{[XA]}$	$m_{[XB]}$	$m_{[Y]}$	$m_{[Z+inter]}$	$m_{[tot]}$	$m_{[abs]}$
Mn ₂ CoAl	5.73	-1.52	2.61	0.98	0.18	2.0	5.29
Ti ₂ CoSi	6.03	1.41	0.71	0.39	0.49	3.0	3.00
Ti ₂ MnAl	6.24	1.13	1.00	-2.59	0.46	0.0	5.18
Ti ₂ VAs	6.23	1.04	0.42	-1.61	0.15	0.0	3.22
Cr ₂ ZnSi	5.85	-1.59	1.64	0.03	-0.08	0.0	3.34

III. RESULTS AND DISCUSSION

This section is divided into three parts. In the first part we discuss the ground state properties and magnetic moments of the studied compounds. The second part deals with the exchange interactions, spin-wave dispersions, as well as spin stiffness constants. The last part focusses on the temperature dependence of the magnetization and critical temperature. Note that Ti₂CoSi presents similar behavior to Mn₂CoAl and Ti₂VAs presents similar properties to Ti₂MnAl. Thus we will focus our discussion mainly on Mn₂CoAl, Ti₂MnAl, and Cr₂ZnSi compounds.

A. Spin gapless semiconducting behavior and magnetic moments

The first step in the study of these materials is to establish their ground state properties at 0 K as obtained from our first-principles calculations. In Fig. 2 we have plotted the density of states (DOS) projected on the transition metal atoms for Mn₂CoAl, Ti₂MnAl and Cr₂ZnSi and in Table I we present the atomic and total spin magnetic moments for all five compounds. We do not present band structure plots since they are known from previous works.^{32,36} In all studied compounds we get a finite gap in the minority-spin band structure (negative values of DOS) and a zero-width gap in the majority-spin band structure. In the case of Mn₂CoAl and Cr₂ZnSi the Fermi level is located at the middle of the minority-spin energy gap and for Ti₂MnAl the Fermi level is located at the left edge of the gap. The position of the Fermi level within the gap is important with respect to the coupling between collective and single electron excitations discussed later. For all five compounds under study the total DOS per formula unit (f.u.) is similar to the ones calculated in Ref. 32 with a different full-potential method and thus spin-gapless semiconducting behavior of these compounds is a robust prediction of ab-initio electronic structure calculations.

Among the five studied compounds, Mn₂CoAl is a fer-

rimagnet and Ti₂CoSi a ferromagnet with total spin magnetic moments per f.u. of 2 and 3 μ_B , respectively, and the other three compounds combine the SGS character to a fully-compensated ferrimagnetic state presenting zero total spin magnetic moments per f.u. as shown in Table I. In the case of the four ferrimagnetic compounds, the X atoms at the B sites couple : either (a) antiferromagnetically to the X atoms at the A sites and ferromagnetically to the Y atoms at the C sites (cases of Mn₂CoAl and Cr₂ZnSi), or (b) ferromagnetically to the X atoms at the A sites and antiferromagnetically to the Y atoms at the C sites (cases of Ti₂MnAl and Ti₂VAs). This behavior is expected from the so-called Bethe-Slater curve.⁶³ The early transition metal atoms like, Cr and Mn, when they are close to each other in space tend to have antiparallel spin magnetic moments. On the other hand for the nearest Ti atoms, the coupling tends to be ferromagnetic (Ti^A and Ti^B atoms in Ti₂YZ compounds). This behavior is also reflected on the exchange constants calculated and presented in the next subsection. Interestingly even in the case of Cr₂ZnSi, where Zn is almost non-magnetic since all its *d*-states are occupied lying below the energy window presented in Fig. 2, the small induced spin magnetic moment at the Zn and Si atoms leads to a small imbalance of the spin moments between the two Cr atoms (Cr^A has as a spin moment of $-1.59 \mu_B$ and Cr^B of $1.64 \mu_B$) and Cr^A resolved DOS presented in Fig. 2 is not an exact mirror image of the Cr^B DOS as in conventional antiferromagnets.

Finally, we should shortly discuss the values of the atomic spin magnetic moments presented in Table I. For all five compounds, spin moments are similar to the results in Ref. 32 where the FPLO⁽⁴⁹⁾ electronic structure code has been employed. Moreover for Mn₂CoAl results agree with the calculated values in Refs. 36–38 and for Ti₂MnAl with the results presented in Ref. 42. Since in each study a different full-potential ab-initio method has been used, we can be confident of the validity of our results. Concerning now the experimentally available data, in Refs. 36 and 38 only the total spin magnetic moment per f.u. for Mn₂CoAl has been measured which has been found to be 1.95 and exactly 2 μ_B , respectively, in agreement with our calculated value of 2 μ_B . A similar total spin magnetic moment (1.94 μ_B) has been measured by Xu and collaborators⁴¹ for Mn₂CoAl films on Si substrates at 5 K. The only discrepancy occurs in the study of Jamer *et al.*⁴⁰ in Mn₂CoAl films on GaAs(001), where X-ray magnetic circular dichroism (XMCD) experiments were carried out. Although XMCD is a powerful technique, in Mn₂CoAl there exist two Mn atoms with opposite spin magnetic moments. XMCD can distinguish between different elements but cannot distinguish atoms of the same chemical element with different spin magnetic moments and thus the values of the Mn moments in Ref. 40 cannot be interpreted as atomic moments. Note that in FLAPW method, the atomic spin magnetic moments are calculated by integrating the spin-dependent charge density within each muffin-tin sphere surrounding

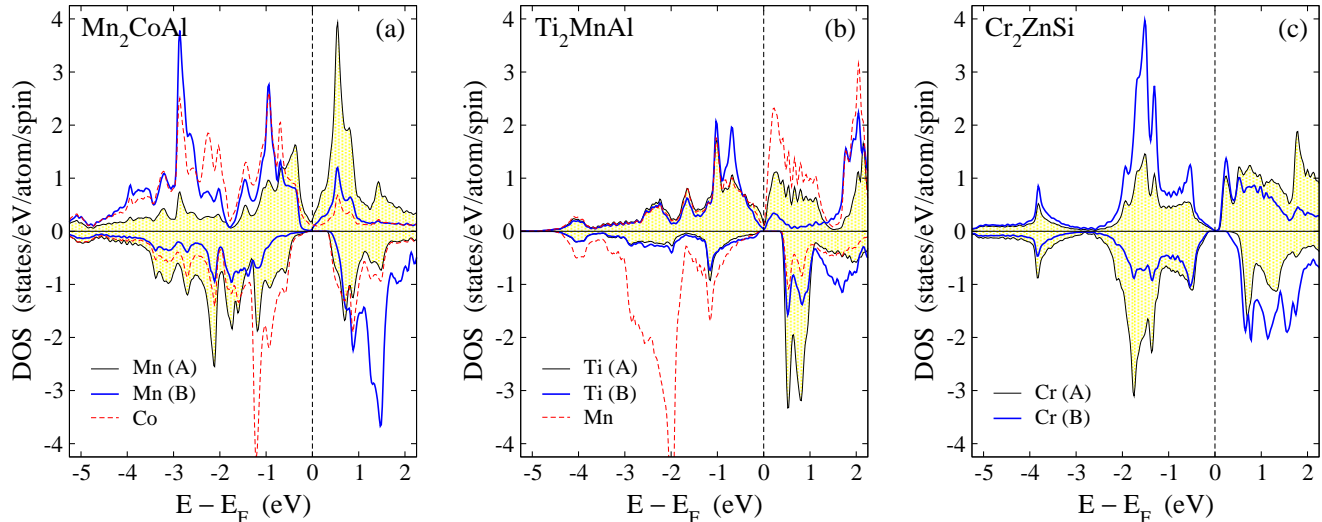


FIG. 2: Density of states (DOS) projected on the transition metal atoms. In the case of Mn_2CoAl , positive (negative) DOS values correspond to the majority (minority) spin electrons. In the case of the other two compounds, which are fully-compensated ferrimagnets, spin-up (positive DOS) and spin-down (negative DOS) electrons have been chosen such that the atomic spin magnetic moments in Table I have the right sign. Fermi level is set to the zero energy value.

each atom. The interstitial region is not assigned to any atom. Although we have used almost touching muffin-tin spheres we can see in Table I that in the case of Ti_2MnAl and Ti_2CoSi a significant part of the spin magnetic moment is located at the interstitial region. This should be attributed to the fact that early transition metals have d -states extending further away from the nucleus compared to late transition metals and the smaller the valence the more extended are the d -states.

B. Exchange interactions and spin-wave dispersion

Our calculations have shown that in the compounds under study inter-sublattice exchange interactions play a dominant role in formation of the magnetic state and critical temperature. In Fig. 3 we present the inter-sublattice exchange constants as a function of distance. Negative values of the exchange constants reflect an antiferromagnetic coupling of the corresponding spin moments and positive values a ferromagnetic coupling. In all compounds the inter-sublattice nearest neighbor interactions dominate and especially the interaction between the X^B atom and its X^A and Y nearest neighbors (Fig. 1). The interactions between next-nearest neighbors X^A and Y are expectedly weaker. In the case of Cr_2ZnSi the Zn atom is almost non magnetic while in the case of Mn_2CoAl the intra-sublattice exchange constants between the Mn^A - Mn^A atoms have a sizeable value despite their large distance. In the case of Ti_2MnAl , the $\text{Ti}^{A,B}$ have positive spin moments and the Mn^C has neg-

ative spin moment as shown in Table I. The situation is different to Mn_2CoAl where Mn^A site has negative, and Mn^B site and Co^C have positive moments. Thus the X^A - X^B and X^B - Y interactions have different signs for the two compounds. We can conclude that for the SGSs under study the interactions are short range: as seen from the Fig. 3 they decay quickly with the distance. This can be attributed to the existence of the finite spin-gap as discussed in literature in detail for half metallic Heusler compounds.^{66,67}

The short range nature of exchange interaction in Mn_2CoAl and similar compounds has been shown by Meinert and collaborators in Ref. 37. Moreover, in the case of Mn_2CoAl our results agree very well with the results obtained in Ref. 37, considering the difference of a pre-factor 1/2 in the definitions of the Heisenberg Hamiltonian between Ref. 37 and the present work. (Also note that in their notations the sequence of the atoms is Co-Mn^B - Mn^C - Al and thus our Mn^A atom corresponds to the Mn^C atom in their article). Further calculations by Wollmann and collaborators on a series of Mn_2 -based inverse Heusler compounds have confirmed the short-range nature of the interactions in these materials.⁴³

The contribution of each type of exchange interaction to the total exchange field J_0 (the Weiss field acting on a spin moment) is given by the sum of the interactions over all possible pairs or, partially, over all pairs within a sublattice. The calculated values for the intra- and inter-sublattice J_0 is presented in Table II. Our results confirm the conclusions drawn in the previous paragraph. The on-site inter-sublattice J_0 are considerably larger than

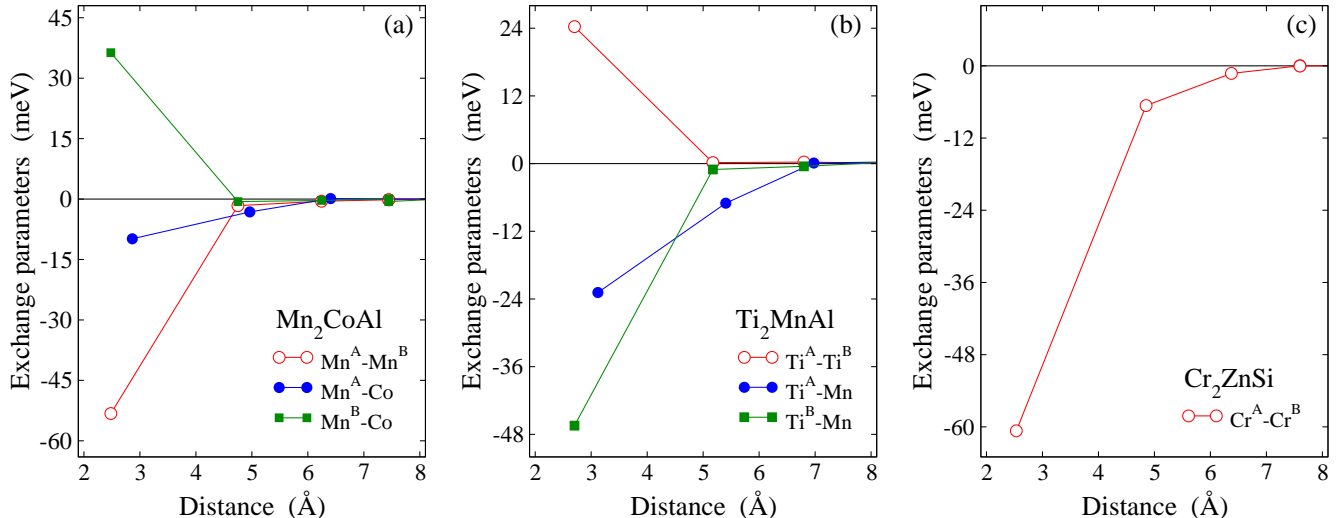


FIG. 3: Inter-sublattice Heisenberg exchange parameters as a function of inter-atomic distances for (a) Mn_2CoAl , (b) Ti_2MnAl , and (c) Cr_2ZnSi .

TABLE II: On-site intra-sublattice (e.g. $J_0^{X^A-X^A} \equiv \sum_{\mathbf{R}} J_{0\mathbf{R}}^{X^A-X^A}$, where \mathbf{R} is the lattice vector) and inter-sublattice (e.g. $J_0^{X^A-X^B} \equiv \sum_{\mathbf{R}} J_{0\mathbf{R}}^{X^A-X^B}$) exchange constants (in meV), spin-wave stiffness constant D (in $\text{meV}\cdot\text{\AA}$ for compensated ferrimagnets or $\text{meV}\cdot\text{\AA}^2$ for ferri- and ferromagnets), and the mean-field and Monte Carlo calculated critical temperatures (in K) for the compounds under study. Note that for the inverse X_2YZ compounds the two X transition metal atoms occupy the A and B sites and the third transition metal atom Y occupies the C site.

Compound	$J_0^{X^A-X^A}$	$J_0^{X^B-X^B}$	J_0^{Y-Y}	$J_0^{X^A-X^B}$	$J_0^{X^A-Y}$	$J_0^{X^B-Y}$	D	T_c^{MFA} (K)	T_c^{MC} (K)
Mn_2CoAl	-73.0	-29.7	-10.5	-238.4	-84.5	132.4	$677 \text{ meV}\cdot\text{\AA}^2$	1134	770
Ti_2CoSi	22.7	6.9	5.22	169.4	69.8	0.6	$636 \text{ meV}\cdot\text{\AA}^2$	766	550
Ti_2MnAl	6.5	1.9	-30.0	101.4	-184.4	-196.8	$274 \text{ meV}\cdot\text{\AA}$	1222	960
Ti_2VAs	37.5	2.3	92.4	45.8	-145.5	-55.1	$598 \text{ meV}\cdot\text{\AA}$	910	800
Cr_2ZnSi	21.2	-18.1	-	-336.4	-	-	$752 \text{ meV}\cdot\text{\AA}$	1308	1040

the intra-sublattice J_0 and only in the case of Mn_2CoAl and Ti_2VAs the $J_0^{\text{Mn}^A-\text{Mn}^A}$ and $J_0^{\text{V}-\text{V}}$ makes a considerable contribution into the total exchange field with different signs.

In Fig. 4 we present the spin-wave dispersion along the high symmetry lines in the Brillouin zone for Mn_2CoAl , Ti_2MnAl and Cr_2ZnSi . Each spectrum has distinct features. First, the number of branches coincides with the number of magnetic atoms in the unit cell and thus we have three branches for Mn_2CoAl and Ti_2MnAl and two branches for Cr_2ZnSi where the Zn atom is not magnetic. The energy dispersion curves of all compounds under study are typical for magnets with short range interactions, where nearest-neighbors and next-nearest-neighbors interactions dominate, and do not yield any instabilities. Instabilities can occur if the acoustic magnon modes have very low energies (close to zero) in some parts of the Brillouin zone but this is not the case for any of

the studied compounds.

In the case of Mn_2CoAl the acoustic branch shows a typical behavior of ferro/ferrimagnets and around the Γ point the energy-dispersion curve shows a quadratic behavior with a spin-wave stiffness constant D of $677 \text{ meV}\cdot\text{\AA}^2$. This value exceeds typical values of transition metal ferromagnets which usually range between 300 and $600 \text{ meV}\cdot\text{\AA}^2$,⁵⁹ and is close to the maximum known values of $715 \text{ meV}\cdot\text{\AA}^2$ for Co_2FeSi ⁶⁴ and $800 \text{ meV}\cdot\text{\AA}^2$ for $\text{Fe}_{53}\text{Co}_{47}$.⁶⁵ Ti_2CoSi as shown in Table II exhibits a D value of $636 \text{ meV}\cdot\text{\AA}^2$ close to the value for Mn_2CoAl .

Although Cr_2ZnSi is not a true antiferromagnet, around the Γ point the energy dispersion is linear and the optical and acoustic branch coincide showing considerable difference only at the plateau close to the Brillouin zone boundary (X, W, L, K points in Fig. 4). The spin-wave stiffness constant as shown in Table II takes a value of $752 \text{ meV}\cdot\text{\AA}$. In the case of Ti_2MnAl the situation is more complicated. Due to the small spin moments of

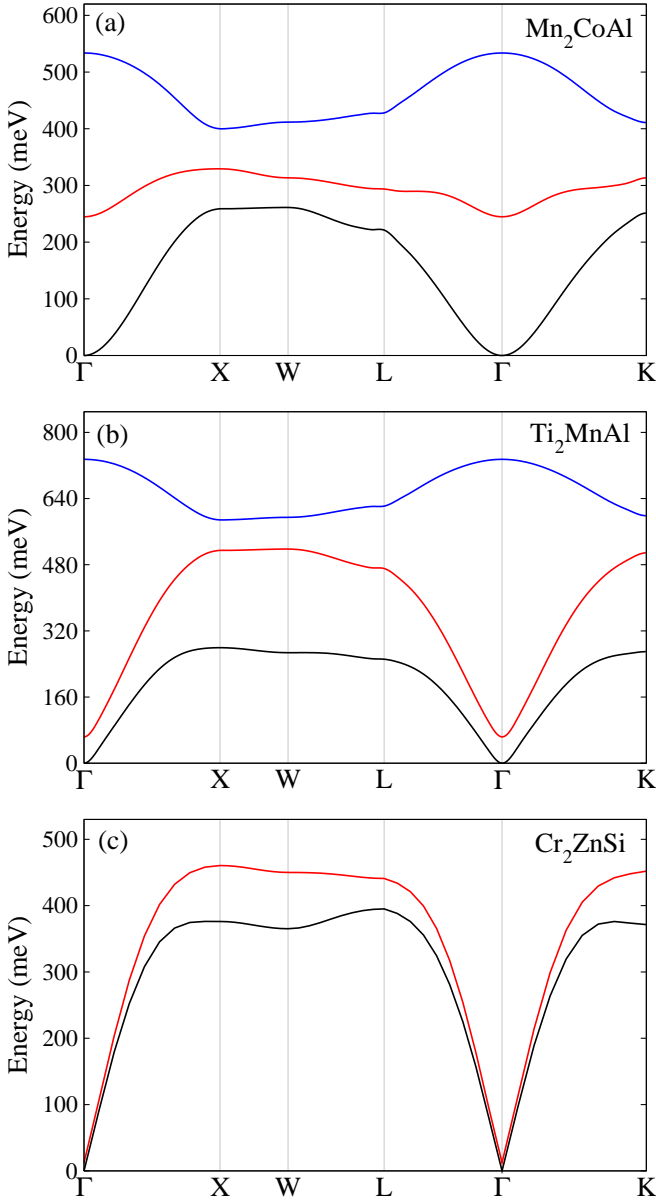


FIG. 4: Spin-wave dispersion curves along the high symmetry lines in Brillouin zone for (a) Mn_2CoAl , (b) Ti_2MnAl , and (c) Cr_2ZnSi . In the case of Mn_2CoAl and Ti_2MnAl , there are three branches since there are three magnetic atoms per unit cell; the sp-atom are almost non-magnetic. In the case of Cr_2ZnSi , the Zn atoms have all their d -valence states completely occupied and have vanishing spin magnetic moments, and thus there are two branches. In the case of Mn_2CoAl the dispersion curve of the acoustic branch around the Γ point shows a quadratic behavior while for Cr_2ZnSi the behavior is linear. In the case of Ti_2MnAl , it is in between.

the Ti atoms around the Γ point the energy-dispersion of the acoustic magnon is practically linear but with a small value of the D constant ($274 \text{ meV}\cdot\text{\AA}$). Ti_2VAs also shows a behavior similar to Ti_2MnAl but now D has a much higher value of $598 \text{ meV}\cdot\text{\AA}$.

C. Temperature dependence of magnetization and T_c

In this section we show the temperature dependence of the magnetization and susceptibility calculated with the classical Monte-Carlo technique. In Fig. 5 we present for Mn_2CoAl , Ti_2MnAl and Cr_2ZnSi the temperature dependence of the sublattice and total magnetization per f.u. First, we compare our results to experiment. We plot for Mn_2CoAl our theoretical results together with the experimental results from the Ref. 38 where the temperature dependence of the total magnetization in a polycrystalline film was measured in a field of 1 T. The agreement between the two data sets is good with one curve falling on top of the other with the exception of the region close to the critical temperature. Our curve shows an abrupt decrease close to our calculated critical temperature of 770 K, while in experiments this sharp decrease is shifted lower in temperature since the measured critical temperature in Ref. 38 is 720 K, slightly smaller than our value. Thus the Monte-Carlo technique, which we employ, accurately describes the temperature dependence of the magnetization, indicating also the accurate determination of the exchange constants.

In the case of Cr_2ZnSi , the picture is that of an antiferromagnet with a total spin magnetic moment being almost equal to zero for all temperatures, since we have ignored the magnetic properties of the Zn atom. In the case of Ti_2MnAl the calculated total magnetization (Fig. 5) is not exactly zero as expected from the first-principles result at 0 K (Table I) but it equals to $-0.46 \mu_B$ due to the spin moment of the Al atom and of the interstitial region which we have ignored in our Monte-Carlo calculations. At and close to room temperature (up to ≈ 400 K), where most devices operate, we find that all three compounds still have sizeable values of the sublattice magnetization. Thus the magnetic properties are not deteriorated although the spin-gapless behavior could be lost at this elevated temperature. For example for Mn_2CoAl at 0 K the Mn^A , Mn^B and Co atoms show a sublattice magnetization of about -1.5 , 2.6 and $1.0 \mu_B$ respectively. At room temperature, these values become -1.3 , 2.3 and $0.8 \mu_B$, showing an absolute-value decrease of 13%, 11% and 18%, respectively. The total magnetization per f.u. decreases from $2.0 \mu_B$ at 0 K to $1.8 \mu_B$ at room temperature showing an even smaller decrease of 10%. Thus the compounds under study are adequate to be employed in spintronic/magnetoelectronic devices.

To estimate the critical temperature T_c^{MC} within the Monte-Carlo technique we have plotted in Fig. 6 the susceptibility χ versus the temperature for all compounds under study. Obtained values are presented in Table II and compared with the mean-field estimation of the critical temperature T_c^{MFA} . As seen for all compounds T_c^{MC} is much lower than the T_c^{MFA} . The difference ranges from 110 K for Ti_2VAs up to 364 K for Mn_2CoAl , while for the other compounds it is around 220-270 K. Note that within MFA, the critical temperature is given by the

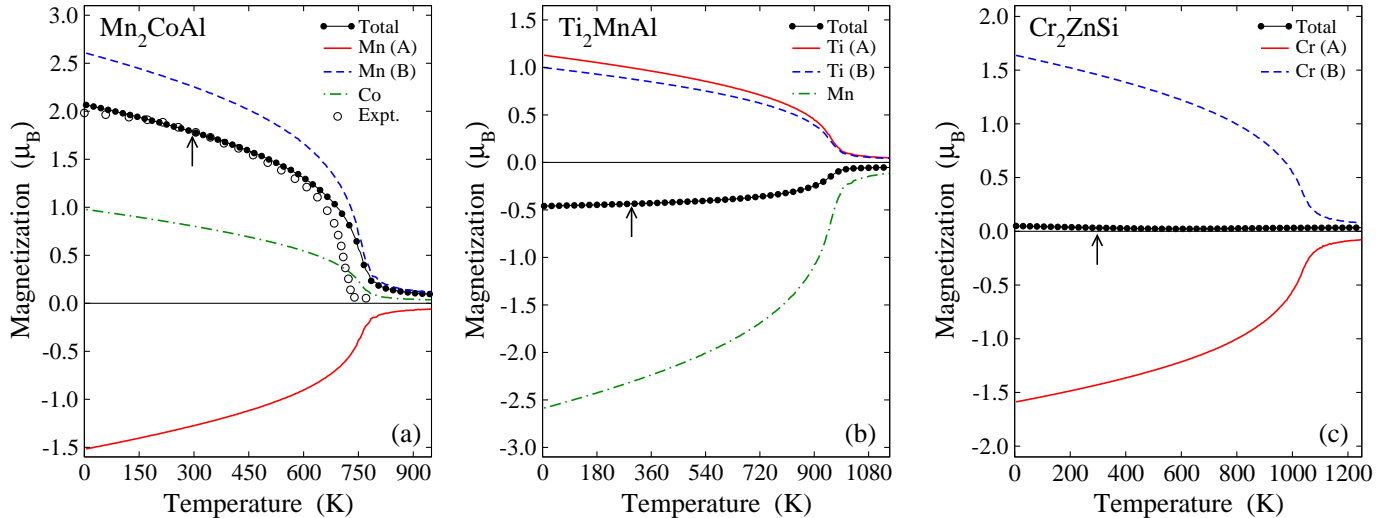


FIG. 5: Calculated temperature dependence of the sublattice and total magnetization for (a) Mn_2CoAl , (b) Ti_2MnAl , and (c) Cr_2ZnSi . In the case of Ti_2MnAl the total spin magnetic moment for 0 K is $-0.46 \mu_B$ since in the Monte-Carlo calculations we ignore the sp-atoms as well as the interstitial region (see Table I). With the arrow we denote the room temperature of 300 K. In the case of Mn_2CoAl we include also the experimental results from Ref. 38.

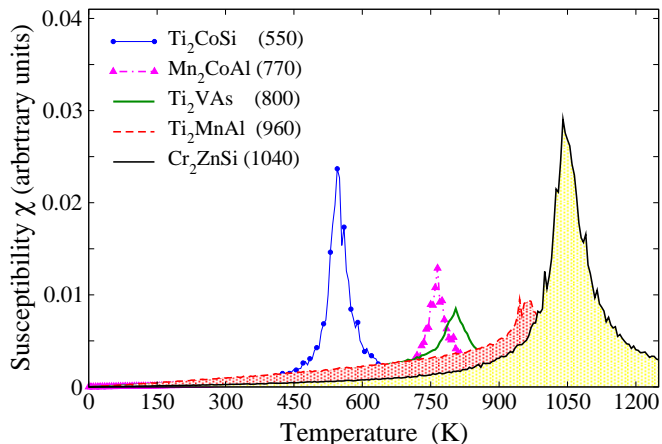


FIG. 6: Calculated temperature dependence of the susceptibility for SGSs. The maximum of the susceptibility corresponds to the critical temperature (shown in parenthesis in the legends).

arithmetic average of all the magnon energy values with equal weight. In reality low-energy magnons have more weight in determining the critical temperature and MFA usually overestimates experimental data by more than 20%.^{58–60} The Monte-Carlo determined critical temperature does not suffer from this drawback and thus it is expected to approach the experimental values of the critical temperature.

In some magnetic compounds, an empirical trend is observed that the critical temperature increases with

the magnitude of the local magnetic moments.^{67–70} This trend is not observed here. The sum of absolute local moments (see Table I) is largest for Mn_2CoAl being $5.29 \mu_B$ but the critical temperature is largest for Cr_2ZnSi for which this sum is only $3.34 \mu_B$. Intuitively we can explain this observation as follows. The critical temperature depends both (a) on the nature of the spin-dependent wavefunction overlap and chemical bonds between nearest neighbors, which is a short-range property and is independent of the magnitude of the spin moments, as well as (b) the more distant interactions which are formed largely because of susceptibility effects (one atom polarizes the Fermi surface electrons and this is felt by a distant atom through the electron propagation) which largely depend on the magnitude of the spin magnetic moments. Here, since the nearest-neighbor interactions are dominant and the long-range ones practically vanish, (a) applies but not (b).

Finally, we compare our values for T_c with experimental and theoretical results on Mn_2CoAl compound. Our calculated MFA and Monte-Carlo values are 1134 K and 770 K, respectively. Meinert and collaborators³⁷ estimated theoretically a $T_c^{\text{MFA}} = 890$ K, smaller than our MFA result. Wollman and collaborators⁴³ calculated $T_c^{\text{MFA}} = 985$ K, in-between our value and the value in Ref. 37 and within the more accurate spherical approximation (SPA)⁴⁴ a value of 740 K, close to our Monte-Carlo value of 770 K.⁴³ Experimentally, for the bulk-like polycrystalline film, Ouadi and collaborators measure for the T_c a value of 720 K,³⁸ while the experiments by Xu and collaborators on thin films of Mn_2CoAl gave a T_c

value of about 550 K;⁴¹ this discrepancy is expected since films present critical temperatures significantly smaller than the bulk samples. Thus our Monte-Carlo value of 770 K is in good agreement both with the SPA calculated value of 740 K of Wollmann *et al.*⁴³ and with the experimental value of 720 K measured by Ouardi *et al.*³⁸

IV. CONCLUSIONS

We employed first principles electronic structure calculations in conjunction with the frozen-magnon method to calculate exchange interactions, spin-wave dispersion, and spin-wave stiffness constants in inverse-Heusler-based spin gapless semiconductor (SGS) compounds Mn_2CoAl , Ti_2MnAl , Cr_2ZnSi , Ti_2CoSi and Ti_2VAs . We find that the magnetic behavior of the SGSs is similar to the half-metallic ferromagnetic full-Heusler alloys, i.e., the inter-sublattice exchange interactions play an essential role in the formation of the magnetic ground state and in determining the critical temperature, T_c . All compounds, except Ti_2CoSi , possess a ferrimagnetic ground state. Due to the finite energy gap in one spin channel, the exchange interactions decay rapidly, and hence magnetism of these SGSs can be described considering only nearest and next-nearest neighbor exchange interactions. The calculated spin-wave dispersion curves are typical for ferrimagnets and ferromagnets, i.e., the number of inequivalent spin-wave branches in the dispersion curves is equal to the number of magnetic atoms in the unit cell. Due to the short range nature of the exchange interac-

tions, the calculated spin-wave stiffness constants turn out to be larger than the elementary $3d$ -ferromagnets.

Calculated exchange parameters are used as input to determine the temperature dependence of the magnetization and the critical temperature T_c of the SGSs. We find that the T_c of all compounds is much above the room temperature. The calculated magnetization curve for Mn_2CoAl as well as the critical temperature are in good agreement with available experimental data.

Our results suggest that, except Mn_2CoAl which has been already synthesized, there are other potential SGS presenting also very high Curie temperatures. In SGS materials, only one spin channel contributes to the transport properties, whereas the other spin channel allows for tunable charge-carrier concentrations. Among the five studied SGS compounds Ti_2MnAl , Ti_2VSi and Cr_2ZnSi present also zero magnetization thus creating vanishing stray fields leading to advantages that have been pointed out for antiferromagnetic spintronic devices.^{74,75} Thus we expect such fully-compensated ferrimagnetic compounds to be more adequate for room temperature spintronic/magnetoelectronic applications based on spin transport.

Acknowledgements

This work was partly supported by the Young Investigators Group Programme of the Helmholtz Association, Germany, contract VH-NG-409. We gratefully acknowledge the support of Jülich Supercomputing Centre (grant jiff38).

* Electronic address: adam.jakobsson@physics.uu.se

† Electronic address: ph.mavropoulos@fz-juelich.de

‡ Electronic address: e.sasioglu@fz-juelich.de

§ Electronic address: galanakis@upatras.gr

¹ P. J. Webster and K. R. A. Ziebeck, in *Alloys and Compounds of d-Elements with Main Group Elements. Part 2*, Edited H. R. J. Wijn, Landolt-Boörnstein, New Series, Group III, Springer-Verlag, Berlin (1988), Vol. 19,Pt.c, pp. 75-184.

² K. R. A. Ziebeck and K.-U. Neumann, in *Magnetic Properties of Metals*, Edited H. R. J. Wijn, Landolt-Börnstein, New Series, Group III, Springer, Berlin (2001), Vol. 32/c, pp. 64-414.

³ F. Heusler, *Verh. Dtsch. Phys. Ges.* **12**, 219 (1903).

⁴ I. Žutić, J. Fabian, and S. Das Sarma, *Rev. Mod. Phys.* **76**, 323 (2004).

⁵ M. I. Katsnelson, V. Yu. Irkhin, L. Chioncel, and A. I. Lichtenstein, and R.A. de Groot, *Rev. Mod. Phys.* **80**, 315 (2008).

⁶ C. Felser, G. H. Fecher, and B. Balke, *Angew. Chem. Int. Ed.* **46**, 668 (2007).

⁷ T. Graf, C. Felser, and S. S. P. Parkin, *Progress in Solid State Chemistry* **39**, 1 (2011).

⁸ R. A. de Groot, F. M. Mueller, P. G. van Engen, and K. H. J. Buschow, *Phys. Rev. Lett.* **50**, 2024 (1983).

⁹ W. E. Pickett and H. Eschrig, *J. Phys.: Condens. Matter* **19**, 315203 (2007).

¹⁰ M. Bowen, A. Barthélémy, M. Bibes, E. Jacquet, J. P. Contour, A. Fert, D. Wortmann, and S. Blügel, *J. Phys.: Condens. Matter* **17**, L407 (2005).

¹¹ I. Galanakis, P. H. Dederichs, and N. Papanikolaou, *Phys. Rev. B* **66**, 134428 (2002).

¹² I. Galanakis, P. H. Dederichs, and N. Papanikolaou, *Phys. Rev. B* **66**, 174429 (2002).

¹³ M. Gillessen and R. Dronskowski, *J. Comput. Chem.* **30**, 1290 (2009).

¹⁴ S. Skafouturos, K. Özdoğan, E. Şaşıoğlu, and I. Galanakis, *Phys. Rev. B* **87**, 024420 (2013).

¹⁵ M. Gillessen and R. Dronskowski, *J. Comput. Chem.* **31**, 612 (2010).

¹⁶ K. Özdoğan, E. Şaşıoğlu, and I. Galanakis, *J. Appl. Phys.* **113**, 193903 (2013).

¹⁷ I. Galanakis, K. Özdoğan, and E. Şaşıoğlu, *Appl. Phys. Lett.* **103**, 142404 (2013).

¹⁸ I. Galanakis, K. Özdoğan, and E. Şaşıoğlu, *J. Phys.: Condens. Matter*, **26**, 086003 (2014).

¹⁹ I. Galanakis and E. Şaşıoğlu, *Appl. Phys. Lett.* **99**, 052509 (2011)

²⁰ H. Y. Jia, X. F. Dai, L. Y. Wang, R. Liu, X. T. Wang, P. P. Li, Y. T. Cui, and G. D. Liu, *J. Magn. Magn. Mater.*

- 367**, 33 (2014).
- 21 A. Hirohata and K. Takanashi, *J. Phys. D: Appl. Phys.* **47**, 193001 (2014).
 - 22 Isaak M. Tsidilkovski, in *Electron Spectrum of Gapless Semiconductors*, edited by Klaus von Klitzing, Springer Series in Solid-State Sciences Vol. 116 (Springer, New York, 1996).
 - 23 X. L. Wang, *Phys. Rev. Lett.* **100**, 156404 (2008).
 - 24 X. Wang, G. Peleckis, C. Zhang, H. Kimura, and S. Dou, *Adv. Mat.* **21**, 2196 (2009).
 - 25 D. H. Kim, J. Hwang, E. Lee, K. J. Lee, S. M. Choo, M. H. Jung, J. Baik, H. J. Shin, B. Kim, K. Kim, B. I. Min, and J.-S. Kang, *Appl. Phys. Lett.* **104**, 022411 (2014).
 - 26 Y. Pan and Z. Yang, *Phys. Rev. B* **82**, 195308 (2010).
 - 27 Y. Pan and Z. Yang, *Chem. Phys. Lett.* **518**, 104 (2011).
 - 28 S.-D. Guo and B.-G. Liu, *J. Phys.: Condens. Matter* **24**, 045502 (2012).
 - 29 Z. F. Wang, S. Jin, and F. Liu, *Phys. Rev. Lett.* **111**, 096803 (2013).
 - 30 J. He, P. Zhou, N. Jiao, L. Z. Sun, X. Chen, and W. Lu, arXiv: 1308.0253 (2013).
 - 31 L. Chioncel, P. Mavropoulos, M. Ležaić, S. Blügel, E. Arrión, M. I. Katsnelson, and A. I. Lichtenstein, *Phys. Rev. Lett.* **96**, 197203 (2006).
 - 32 S. Skaftouros, K. Özdoğan, E. Şaşıoğlu, and I. Galanakis, *Appl. Phys. Lett.* **102**, 022402 (2013).
 - 33 G. Z. Xu, E. K. Liu, Y. Du, G. J. Li, G. D. Liu, W. H. Wang, and G. H. Wu, *Europhys. Lett.* **102**, 17007 (2013).
 - 34 G. Y. Gao and K.-L. Yao, *Appl. Phys. Lett.* **103**, 232409 (2013).
 - 35 L. Bainsla, A. I. Mallick, M. Manivel Raja, A. K. Nigam, B. S. D. Ch. S. Varaprasad, Y. K. Takahashi, A. Alam, K. G. Suresh, and K. Hono, *Phys. Rev. B* **91**, 104408 (2015).
 - 36 G. D. Liu, X. F. Dai, H. Y. Liu, J. L. Chen, Y. X. Li, Gang Xiao, and G. H. Wu, *Phys. Rev. B* **77**, 014424 (2008).
 - 37 M. Meinert, J. Schmalhorst, and G. Reiss, *J. Phys.: Condens. Matter* **23**, 036001 (2011).
 - 38 S. Ouardi, G. H. Fecher, C. Felser, and J. Kübler, *Phys. Rev. Lett.* **110**, 100401 (2013).
 - 39 M. E. Jamer, B. A. Assaf, T. Devakul, and D. Heiman, *Appl. Phys. Lett.* **103**, 142403 (2013).
 - 40 M. E. Jamer, B. A. Assaf, G. E. Sterbinsky, D. A. Arena, and D. Heiman, *J. Appl. Phys.* **116**, 213914 (2014).
 - 41 G. Z. Xu, Y. Du, X. M. Zhang, H. G. Zhang, E. K. Liu, W. H. Wang, and G. H. Wu, *Appl. Phys. Lett.* **104**, 242408 (2014).
 - 42 H. Y. Jia, X. F. Dai, L. Y. Wang, R. Liu, X. T. Wang, P. P. Li, Y. T. Cui, and G. D. Liu, *AIP Advances* **4**, 047113 (2014).
 - 43 L. Wollmann, S. Chadov, J. Kübler, and C. Felser, *Phys. Rev. B* **90**, 214420 (2014).
 - 44 T. Moriya, *Spin Fluctuations in Itinerant Electron Magnetism*, Springer Series in Solid-State Sciences No. 56 (Springer, Berlin/Heidelberg, 1985).
 - 45 I. Galanakis, K. Özdoğan, E. Şaşıoğlu, and S. Blügel *J. Appl. Phys.* **115**, 093908 (2014).
 - 46 Y. J. Zhang, G. J. Li, E. K. Liu, J. L. Chen, W. H. Wang, and G. H. Wu, *J. Appl. Phys.* **113**, 123901 (2013).
 - 47 J. Kudrnovský, V. Drchal, and I. Turek, *Phys. Rev. B* **88**, 014422 (2013).
 - 48 N. Metropolis, A. W. Rosenbluth, M. N. Rosenbluth, A. H. Teller, and E. Teller, *J. Chem. Phys.* **21**, 1087 (1953).
 - 49 K. Koepf and H. Eschrig, *Phys. Rev. B* **59**, 1743 (1999).
 - 50 J. P. Perdew, K. Burke, and M. Ernzerhof, *Phys. Rev. Lett.* **77**, 3865 (1996)
 - 51 <http://www.flapw.de>
 - 52 A. Oswald, R. Zeller, and P. H. Dederichs, *J. Phys. F: Met. Phys.* **15**, 193 (1985).
 - 53 P. Bruno, *Phys. Rev. Lett.* **90**, 087205 (2003).
 - 54 N. M. Rosengaard and B. Johansson, *Phys. Rev. B* **55**, 14975 (1997).
 - 55 S. V. Halilov, H. Eschrig, A. Ya. Perlov, and P. M. Oppeneer, *Phys. Rev. B* **58**, 293 (1998).
 - 56 L. M. Sandratskii and P. Bruno, *Phys. Rev. B* **67**, 214402 (2003).
 - 57 A. Jakobsson, B. Sanyal, M. Ležaić, and S. Blügel, *Phys. Rev. B* **88**, 134427 (2013).
 - 58 E. Şaşıoğlu, L. M. Sandratskii, P. Bruno, and I. Galanakis, *Phys. Rev. B* **72**, 184415 (2005).
 - 59 M. Pajda, J. Kudrnovský, I. Turek, V. Drchal, P. Bruno, *Phys. Rev. B* **64**, 174402 (2001).
 - 60 E. Şaşıoğlu, L. M. Sandratskii, and P. Bruno, *J. Appl. Phys.* **98**, 063523 (2005).
 - 61 E. Şaşıoğlu, L. M. Sandratskii, and P. Bruno, *Phys. Rev. B* **70**, 024427 (2004).
 - 62 Anderson P W, *Theory of magnetic exchange interactions: Exchange in insulators and semiconductors*, in *Solid State Physics*, edited by F. Seitz and D. Turnbull (Academic Press, New York), Vol. 14 pp. 99-214.
 - 63 D. Jiles, *Introduction to Magnetism and Magnetic Materials*, (Chapman & Hall, London, 1998).
 - 64 O. Gaier, J. Hamrle, S. Trudel, B. Hillebrands, H. Schneider, and G. Jakob, *J. Phys. D: Appl. Phys.* **42**, 232001 (2009).
 - 65 X. Liu, R. Sooryakumar, C. J. Gutierrez, and G. A. Prinz, *J. Appl. Phys.* **75**, 7021 (1994).
 - 66 M. Pajda, J. Kudrnovský, I. Turek, V. Drchal, and P. Bruno, *Phys. Rev. B* **64**, 174402 (2001).
 - 67 J. Ruzs, L. Bergqvist, J. Kudrnovsky, and I. Turek, *Phys. Rev. B* **73**, 214412 (2006).
 - 68 J. Kübler, G. H. Fecher, and C. Felser, *Phys. Rev. B* **76**, 024414 (2007).
 - 69 E. Şaşıoğlu, L. M. Sandratskii and P. Bruno, *J. Phys.: Condens. Matter* **17**, 995 (2005).
 - 70 E. Şaşıoğlu, *Phys. Rev. B* **79**, 100406(R) (2009).
 - 71 D. P. Landau and K. Binder, *A Guide to Monte Carlo Simulations in Statistical Physics* (Cambridge University Press, Cambridge, 2000).
 - 72 M. Matsumoto and T. Nishimura, *ACM Trans. Model. Comput. Simul.* **8**, 3 (1998).
 - 73 M. Ležaić, P. Mavropoulos, G. Bihlmayer, and S. Blügel, *Phys. Rev. B* **88**, 134403 (2013).
 - 74 A. S. Núñez, R. A. Duine, P. Haney, and A. H. MacDonald, *Phys. Rev. B* **73**, 214426 (2006).
 - 75 A. B. Shick, S. Khmelevskiy, O. N. Mryasov, J. Wunderlich, and T. Jungwirth, *Phys. Rev. B* **81**, 212409 (2010).